PERGAMON

PII: S1359-6454(98)00380-2

Acta mater. Vol. 47, No. 3, pp. 971–982, 1999

Printed in Great Britain
1359-6454/99 $19.00 + 0.00

THREE-DIMENSIONAL MODELING OF EQUIAXED DENDRITIC GROWTH ON A MESOSCOPIC SCALE

I. STEINBACH[1], C. BECKERMANN[2], B. KAUERAUF[1]†, Q. LI[2] and J. GUO[2]

[1]ACCESS e.V., D-52056 Aachen, Germany and [2]Department of Mechanical Engineering, The University of Iowa, Iowa City, IA 52242-1527, U.S.A.

(Received 13 May 1998; accepted in revised form 29 October 1998; accepted 1 November 1998)

Abstract—A novel mesoscopic modeling technique has been developed to simulate the unsteady growth of multiple equiaxed dendritic grains into a supercooled melt of a pure substance. In the model, the numerical calculation of the temperature field in the supercooled melt between the grains is coupled with a stagnant-film model for dendrite tip growth, such that without resolving individual dendrite arms the evolution of the grain envelope and the internal solid fraction can be predicted. The simulations are in good agreement with experiments for the growth of a single dendritic grain of the model substance succinonitrile. The model is then applied to simulate the growth of various configurations of up to 14 strongly interacting grains. The results indicate that the use of local analytical solutions in numerical calculations is a viable technique for simulating large-scale dendritic growth phenomena. © *1999 Acta Metallurgica Inc. Published by Elsevier Science Ltd. All rights reserved.*

1. INTRODUCTION

Dendrites are the most common growth morphology in solidification of metals, alloys, and other substances [1]. Dendritic growth is characterized by the propagation of a primary tip and the nonlinear evolution of secondary and tertiary side-branches on a microscopic scale (from 10^{-6} to 10^{-5} m). Equiaxed grains result if the growth is from free nuclei into a supercooled melt. An assemblage of many equiaxed dendritic grains constitutes a so-called mushy zone on a macroscopic scale (10^{-1} m). Modeling of equiaxed dendritic solidification on the scale of a typical mushy zone thus requires the simultaneous consideration of growth and transport phenomena over length scales ranging over roughly five orders of magnitude. The mesoscopic scale is defined here as being between the microscopic and macroscopic length scales, and is of the order of from 10^{-4} to 10^{-3} m. A mesoscopic unit cell inside a mush would typically contain of the order of 10 equiaxed grains and literally thousands of dendrite arms and tips. Such unit cells or representative elementary volumes (REVs) form the basic building blocks of macroscopic or volume-averaged solidification models used in the simulation of casting processes [2]. Accurate modeling of the dendritic growth processes inside a mesoscopic unit cell is not only important for the prediction of the final grain structure of a solidified material, but also for feeding local information (e.g. latent heat evolution, solute rejection) back to the macroscopic model. The development of a model for simulating the growth of an assemblage of equiaxed dendritic grains on a mesoscopic scale is the objective of the present study. Of primary interest are prediction of the evolution of the grain shapes, the growth interactions between multiple grains, and the nature of the thermal field in the melt between the dendrites. For example, for strongly overlapping thermal fields in front of the dendrite tips of neighboring grains, the tip velocities can be expected to be reduced, up to a point where a globulitic (or spheroidal) grain structure results. On the other hand, for weak interactions the tip velocities will be similar to those for dendrite growth into an infinite melt [3].

The direct numerical simulation of dendritic growth inside a mesoscopic unit cell cannot be achieved with presently available computational power, because the range of length scales that need to be resolved is too large. A recent example illustrating the present limits of direct numerical microstructure simulation is the fully resolved, three-dimensional calculation of dendritic growth by Karma and Rappel [4] using the phase-field method. Their results are limited to a relatively small equiaxed grain, without a full side-branch structure, and relatively high dimensionless supercoolings. The extension to fully dendritic grains growing at the low supercoolings typical of casting processes would require an increase in computational power by at least three orders of magnitude in both speed and memory. On the other end of the spectrum, relatively simple approximate and one-dimensional unit cell models of equiaxed dendritic solidification have been proposed [2, 5] that are

†To whom all correspondence should be addressed.

primarily intended for the prediction of the latent heat evolution during recalescence. Obviously, these models are unable to resolve the actual shape of the growing grains and the internal structure of the mush. One bridge over the gap between direct microscopic simulation and the one-dimensional unit cell models is the so-called cellular automaton modeling of grain growth by Gandin and Rappaz [6]. In this method, the orientation and evolution of the shape of the growing grains is tracked numerically, allowing for a prediction of the final grain structure in a solidified part. However, in a manner similar to the one-dimensional unit cell models, the dendrite growth velocities are calculated based on some local mean supercooling, and the temperature (or concentration) field between the grains is not resolved. Consequently, the cellular automaton model does not allow for a detailed study of the local growth interactions.

The modeling of equiaxed dendritic solidification on a mesoscopic scale in the present study is facilitated by a novel approach that combines a numerical solution of the relevant transport equation (i.e. the heat diffusion equation) on the mesoscopic scale with a local analytical solution of the dendrite tip growth problem at the smallest length scale [7]. With this method, the computational power requirements are reduced by at least three orders of magnitude compared to direct microstructure simulation on a microscopic scale. In general, the use of a local analytical solution or empirical relation in a numerical simulation rests on the notion that the system behavior at the smallest length scale is "universal" and independent of the longer range interactions. Such an approach is commonly utilized in the modeling of turbulent fluid flow, where the effect of the smallest eddies on the mean flow is represented by relatively simple relations that are valid for a large variety of flows. One of the earliest examples is the mixing-length theory [8], which is based on the assumption that the finest-scale turbulence structure is similar everywhere throughout the flow field. Another example is the use of the "universal" law-of-the-wall in modeling various turbulent wall shear flows [8]. The law-of-the-wall is applied in a thin "inner" layer along the surface of a body, corresponding to a few grid points in a numerical simulation, and matched with the mean velocity field in the "outer" region away from the wall, which is obtained from a solution of the relevant transport equations on the system scale. The key point is that the same law-of-the-wall can be used for large variations in the outer flow. Similarly, in the present model, the same analytical relation is employed for all (active) dendrite tips to describe the growth behavior on the smallest length scale, and this relation is then matched with the outer temperature field. The use of this fundamental concept in modeling dendritic solidification has not been attempted before, but seems to be a plausible idea given the large separation of length scales in a dendritic mush. While the present study focuses on the development of the basic model for equiaxed dendritic solidification of a pure substance, an extension to alloys and other growth structures will be straightforward.

The model and the numerical solution procedures are described in the Sections 2 and 3. Then Sections 4 and 5 provide results for a single equiaxed grain and a comparison of the predictions with available experimental data. Then, in Section 6, numerical results are presented for the growth of various configurations of up to 14 interacting grains, which is followed by the conclusions in Section 7.

2. MODEL AND GOVERNING EQUATIONS

A schematic illustration of the various length scales present in equiaxed dendritic growth is shown in Fig. 1(a). The smallest, microscopic length scale is denoted by δ_1, and is of the order of the dendrite tip radii (from 10^{-6} to 10^{-5} m). The dendrite tips grow into the supercooled melt surrounding the grain. The diffusion boundary layers around the tips have a thickness of the same order as the tip radii. The prediction of the tip growth speeds and radii requires the resolution of the thermal field on the scale δ_1, something we accomplish in the present model using a local analytical solution (see below). The mesoscopic scale δ_2 is of the order of

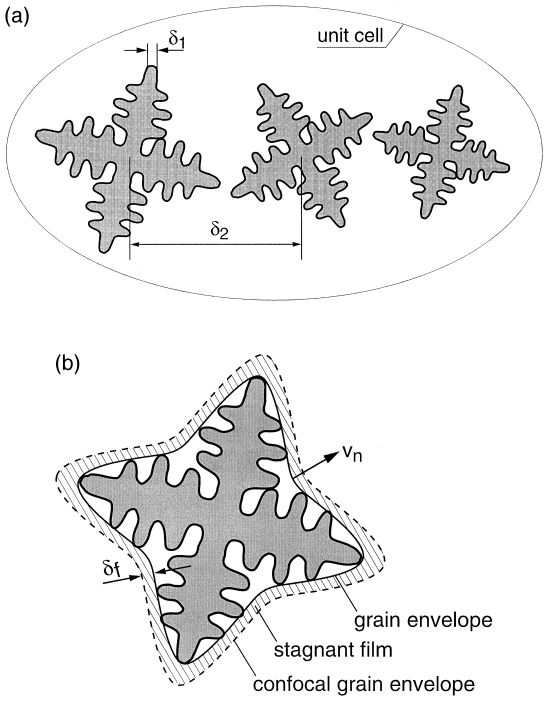

Fig. 1. Schematic illustration of equiaxed dendritic growth: (a) unit cell, where δ_1 is the microscopic scale and δ_2 is the mesoscopic scale; (b) grain envelope and stagnant film.

the spacing between the grains, which is typically two orders of magnitude greater than δ_1. The prediction of the overall shape of a grain and the growth interactions between the grains inside the unit cell requires the resolution of the thermal field on the scale δ_2, which is done here by solving numerically the transient, three-dimensional heat equation in the supercooled melt.

Central to the coupling of the microscopic and mesoscopic transport processes in the present model is the definition of a grain envelope, in a manner similar to previous models [2, 5, 6]. As shown in Fig. 1(b), the grain envelope is a smooth surface connecting the tips of all "active" or "surviving" dendrite branches, where a branch is judged as active when it is longer than the next active branch closer to the primary tip. Therefore, the growth velocities of the grain envelope can be obtained from dendrite tip speeds, as described below. Note that the volume inside the grain envelope contains finely "dispersed" solid and melt. The temperature of the solid/liquid mixture inside this very form-fitting envelope can safely be assumed to be at the melting point, T_m. Consequently, all growth takes place at the envelope surface and the latent heat is conducted into the supercooled melt between the grains.

The local analytical solution used to resolve the temperature field on the microscopic scale δ_1 is the so-called "stagnant-film" modification by Cantor and Vogel [9] of the well-known Ivantsov solution of the heat flow problem around a growing, isothermal paraboloid of revolution representing a dendrite tip. When coupled with a selection criterion [2], this solution provides both the dendrite tip speed, v, and radius, R, as a function of the supercooling ΔT. The regular Ivantsov solution cannot be used because it is only valid when the melt is infinite in extent. In the stagnant-film solution, the supercooling is instead applied at a confocal isothermal paraboloid located a finite distance δ_f away from the dendrite tip and moving with the same speed as the tip. The stagnant-film solution is given by [9]

$$\Delta T = \frac{L}{c} Pe \exp(Pe) \times \left\{ E_1(Pe) - E_1\left[Pe\left(1 + 2\frac{\delta_f}{R}\right)\right]\right\} \quad (1)$$

where ΔT is the supercooling across the stagnant film of thickness δ_f, $Pe = vR/(2\alpha)$ is the tip Peclet number, α is the thermal diffusivity, L is the latent heat, c is the specific heat, and E_1 is the exponential integral function. The selection criterion needed in addition to equation (1) to obtain a unique value of the tip speed can be written as [2]

$$R^2 v = \frac{2\alpha\Gamma}{\sigma^* L/c} \quad (2)$$

where Γ is the Gibbs–Thomson coefficient and σ^* is a selection constant. Combining equations (1) and (2) to provide an explicit relation of the form $v = f(\Delta T)$ can be accomplished by numerical inversion and curve fitting. It is important to realize that this local analytical solution is only used on the microscopic scale, δ_1. Hence, the film thickness, δ_f, is chosen to be of the same order of magnitude as, but greater than the tip radius R. For $\delta_f \gg R$, equation (1) would reduce to the Ivantsov solution.

For a given supercooling across the film, the above local analytical solution can be used to calculate the speeds of every active (primary and secondary) dendrite tip. Because the exact locations of the dendrite side-branches are not known and the grain envelope is a continuous surface, the tip speeds are calculated for every point on the envelope. For this purpose, the same film thickness δ_f is chosen for all tips. Then, as shown in Fig. 1(b), a confocal grain envelope can be defined that is located the distance δ_f away from the regular grain envelope. As opposed to the regular grain envelope, the temperature of the confocal envelope, T_{ce}, is not uniform, because the tip speeds or, equivalently, the supercoolings across the film, $\Delta T = T_m - T_{ce}$, are different for every active dendrite tip. The distribution of T_{ce} is obtained from the numerical solution of the heat equation on the mesoscopic scale, as explained below. Note that the choice of a uniform δ_f leading to the definition of the confocal grain envelope is simply a matter of convenience in the numerical algorithm, and one could have chosen a variable δ_f corresponding to an isothermal confocal envelope. For later use, the tip speeds are converted to normal envelope velocities, v_n, using the following relation

$$\mathbf{v}_n = v\mathbf{n} \cdot \cos\theta \quad (3)$$

where $\mathbf{n}$ is the exterior normal to the envelope and θ is the angle between the normal and the growth axis of the closest dendrite arm. The calculation of the normal is described in the next section. The angle is obtained by specifying the crystallographic orientation of the grain and assuming cubic anisotropy.

The temperature distribution on the mesoscopic scale, δ_2, is obtained by solving numerically the following transient, three-dimensional heat diffusion equation in the supercooled melt between the grain envelopes in the unit cell:

$$\frac{\partial T}{\partial t} = \alpha \nabla^2 T \quad (4)$$

The boundary conditions are the fixed melting temperature, T_m, at (and inside) the moving grain envelope and an adiabatic unit cell. Initially, the melt is taken to be at a uniform temperature T_∞ corresponding to an initial supercooling of $\Delta T_i = T_m - T_\infty$.

As mentioned above, the numerical solution of the heat equation provides the confocal grain envelope temperature distribution, which can formally be written as

$$T_{ce} = T|_{\text{confocal envelope}} \tag{5}$$

Furthermore, the knowledge of the temperature gradient at the envelope from the numerical solution allows for the calculation of the fraction of solid, f_s, formed at the envelope using the following energy balance:

$$-\alpha \frac{\partial T}{\partial n}\bigg|_{\text{envelope}} = \rho \frac{L}{c} |\mathbf{v}_n| f_s \tag{6}$$

Because the envelope continually propagates in an outward direction and the temperature gradient varies with both time and location on the envelope, the solution of equation (6) will establish a certain solid fraction distribution within the grain.

The overall structure of the mesoscopic model as stated above is summarized in Fig. 2, which shows a schematic of the temperature profile normal to a grain envelope. The local analytical solution is used to resolve the temperature profile in the stagnant film for the calculation of the dendrite tip/grain envelope velocity, while the numerical solution of the heat equation provides the temperature distribution on the mesoscopic scale outside of the grain envelope and also the confocal envelope temperature. The two solutions are matched both at the regular and the confocal grain envelope. The numerical solution should only be viewed as an approximation in the film region, because it does not resolve the microscopic temperature field around individual dendrite tips. Proper matching of the analytical and numerical solutions depends primarily on the choice of the film thickness, δ_f. If the film thickness is too small, the steep microscopic temperature gradients near the dendrite tips are not well approximated by the numerical solution on the mesoscopic scale. If, on the other hand, the film thickness is too large, the local analytical solution can become invalid due to thermal fields from neighboring dendrite branches and other grains penetrating into the film. Nonetheless, the relatively large separation of the length scales δ_1 and δ_2 enables one to find a film thickness that works for a reasonably wide range of supercoolings, which is demonstrated below.

3. NUMERICAL SOLUTION PROCEDURES

The numerical method used to solve the model equations consists of two parts: the envelope propagation algorithm and the solution of the heat diffusion equation. The coupling of both establishes the solution of the mesoscopic model.

Equations (1)–(3) provide the normal grain envelope velocity, $\mathbf{v}_n$, as a function of the supercooling across the film. In order to propagate the envelope across the regular and fixed numerical grid, we use a phase-field-like algorithm [10]. A field variable, ϕ, is introduced that varies across the film from 1 in the grain near the envelope to 0 in the supercooled melt away from the confocal envelope. It should be emphasized that this field variable is simply used as an indicator function for purely numerical reasons, and has no physical meaning. The grain envelope is assigned a value of $\phi = 0.95$, while the confocal envelope is placed at $\phi = 0.5$. The transition region for ϕ, defined as the distance δ_ϕ over which ϕ varies from 0.05 to 0.95, is chosen to be twice the film thickness δ_f. The field variable ϕ allows for the calculation of the normal to the envelope according to

$$\mathbf{n} = -\frac{\nabla \phi}{|\nabla \phi|} \tag{7}$$

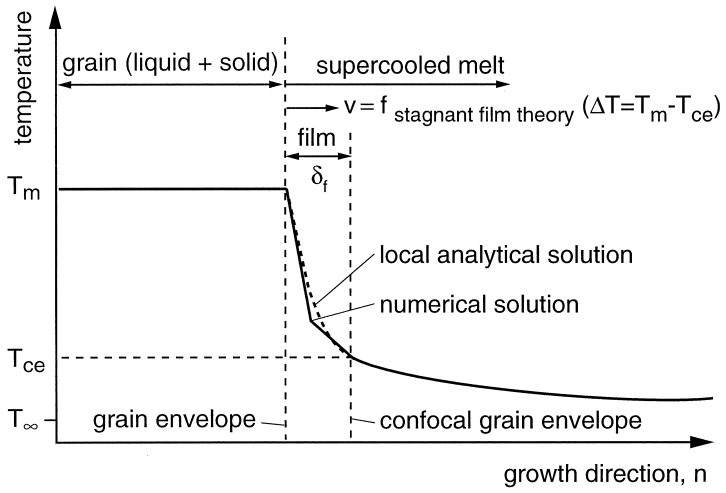

Fig. 2. One-dimensional temperature distribution normal to a grain envelope illustrating the matching of the numerical solution and the local analytical solution at the stagnant film.

The propagation of f is given by

$$\dot{\phi} = \frac{36}{\delta_\phi}\phi^2(1-\phi)^2\left|\mathbf{v}_n(\Delta T)\right| + \mathrm{stab}(\phi) \qquad (8)$$

where the dot above ϕ denotes the time derivative and stab(ϕ) is a stabilization operator. This operator acts as an anti-diffusion flux to keep the ϕ-profile compact and is given by

$$\mathrm{stab}(\phi) = C\left[\frac{\delta_\phi^2}{72}\mathbf{n}\cdot\nabla|\nabla\phi| - \phi(1-\phi)\left(\frac{1}{2}-\phi\right)\right] \qquad (9)$$

where C is a stabilization constant. Taking $C \approx 0.1/\Delta t$ results in magnitudes of the anti-diffusion fluxes that work for any time increment Δt. The ϕ-profile is compact when stab(ϕ) = 0, which leads to the following stable profile of ϕ in the normal direction n

$$\phi(n) = \frac{1}{2}\left(1 - \tanh\frac{3n}{\delta}\right) \qquad (10)$$

Again, the basic structure of the above equations is essentially borrowed from the phase-field method [10] and found to work well as a propagation algorithm for the grain envelope. The formulation ensures that the envelope is a smooth surface and is propagated at the correct velocity regardless of the orientation of the ϕ-surfaces (i.e. the grain) with respect to the grid. Equation (8) is solved using standard finite differences. The grid is uniform and chosen such that at least two grid points lie within the film of thickness δ_f.

The heat diffusion equation, equation (4), is solved using a standard control volume discretization technique. The temperatures of all cells inside the grain envelope, i.e. all cells with $\phi \geq 0.95$, are set to the melting temperature, T_m. The confocal envelope temperatures, T_{ce}, are obtained from the calculated temperature field by interpolation to $\phi = 0.5$. Finally, equation (6) is discretized and solved at each time step to update the solid fraction distribution in the grains.

4. RESULTS FOR A SINGLE GRAIN

Before validating the mesoscopic model using experimental data and studying the growth interactions of multiple grains inside a unit cell, it is useful to examine the predictions from the model for the limiting case of a single grain growing into an essentially infinite melt (i.e. uniform far-field supercooling). This discussion is intended to clarify the coupling between the local analytical solution and the numerical solution of the heat equation, and shed light on the proper choice of the film thickness δ_f. All thermophysical properties are taken to be those of the commonly used metal-model material succinonitrile (SCN), mainly because experimental data are available for this material and the selection constant, σ^*, is reasonably well known [11–13].

As a first test, the mesoscopic model is used to predict the tip velocity of a single dendrite arm. In this limiting case, the Ivantsov theory, coupled with the selection criterion, provides an analytical prediction of the tip speed. A comparison between the theoretical prediction and the calculations is shown in Fig. 3(a). The open squares correspond to mesoscopic model calculations with a film thickness of 200 μm and a grid spacing of 100 μm. It can be seen that the model results are in reasonable agreement with the theory for supercoolings ranging from 0.2 to 1.0 K. It is important to note that the tip radius varies significantly—from 112 μm (at

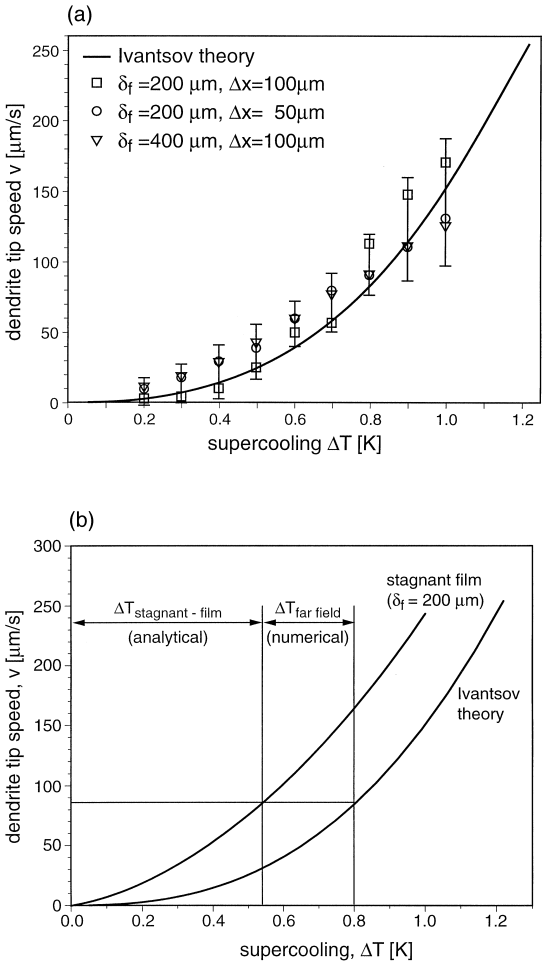

Fig. 3. Predicted results for a single dendrite (SCN) growing into a uniform supercooling: (a) comparison of predicted dendrite tip speeds for various supercoolings with the Ivantsov theory; □ show the results for a film thickness of 200 μm and a grid spacing of 100 μm; the error bars correspond to variation in the grid spacing from 100 μm to 50 μm (○) and to variation in the film thickness from 200 μm to 400 μm (□); (b) partitioning of the total supercooling between the stagnant film and the melt outside the confocal envelope as a function of the dendrite tip speed.

0.2 K) to 15 μm (at 1.0 K)—in this supercooling range. Nonetheless, the film thickness of 200 μm gives good results over the entire range. The agreement somewhat deteriorates above 0.8 K, which can be attributed to the film thickness becoming too large relative to the tip radius. As mentioned earlier, the film thickness should generally be of the same order of magnitude as, but larger than the tip radius, for the use of the local analytical solution to be meaningful. A series of calculations was performed in order to investigate in more detail the sensitivity of the results to the numerical grid

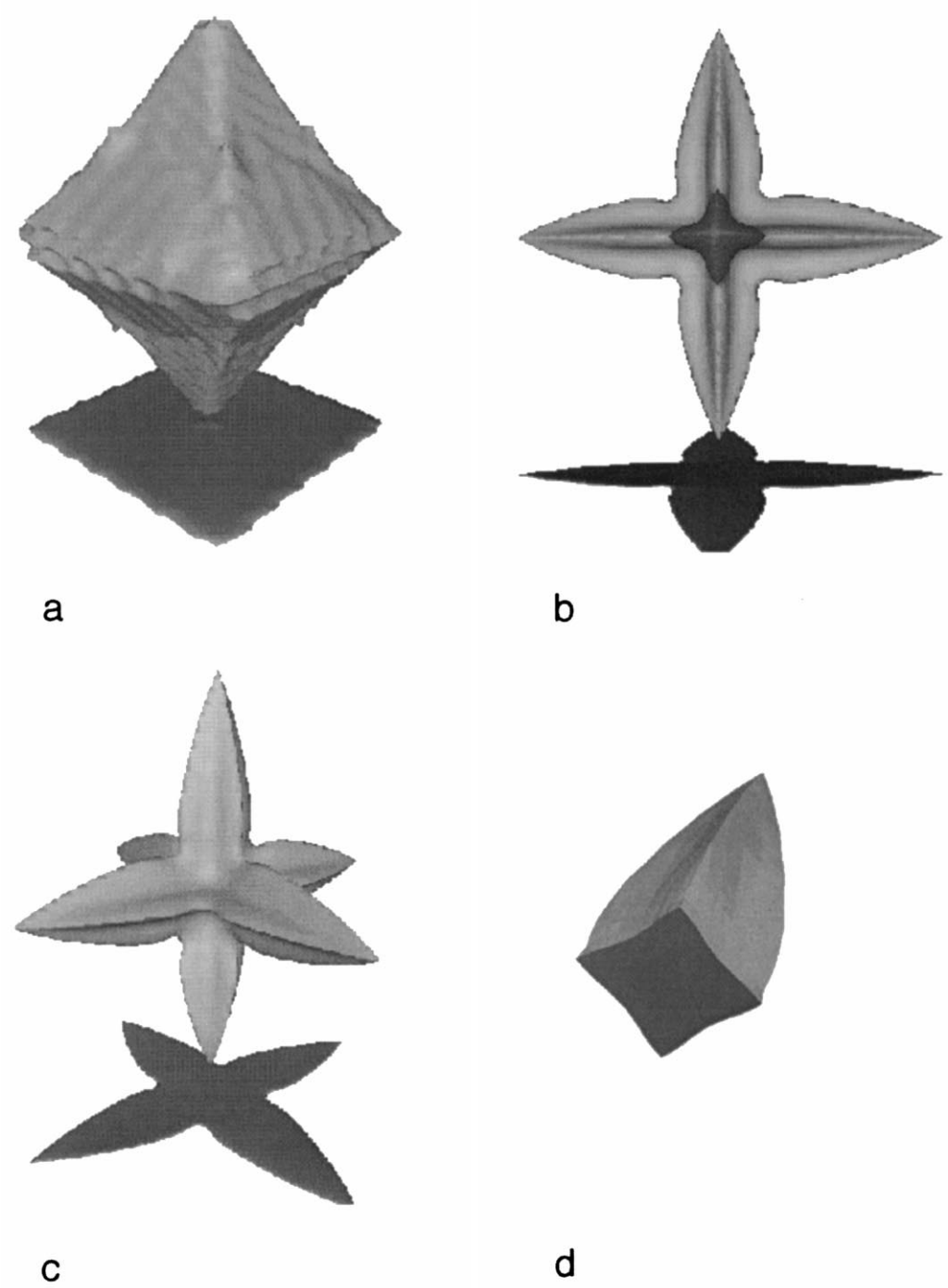

Fig. 4. Predicted envelope shape for a single equiaxed grain growing into a uniform supercooling: (a) octahedric shape that results when the heat diffusion equation is not solved and all dendrite tips grow at the same velocity; (b) and (c) two views of a fully coupled prediction; (d) cut through a primary branch of the grain depicted in (b) and (c).

spacing and the film thickness. The error bars in Fig. 3(a) were obtained by varying the grid spacing by a factor of two, i.e. from 100 μm to 50 μm, while keeping the film thickness constant at 200 μm and by varying the film thickness by a factor of two, i.e. from 200 μm to 400 μm, while keeping the grid spacing constant at 100 μm. The resulting tip speeds vary up to ±25%. Note that a film thickness of 400 μm in one variation is more than 25 times greater than the tip radius at 1.0 K. Such a large ratio is, of course, not recommended.

The partitioning of the total supercooling is further illustrated in Fig. 3(b) for the same conditions as in Fig. 3(a). A film thickness of 200 μm implies that up to a distance of 200 μm from the dendrite tip, the temperature field is resolved by the local analytical solution, while beyond 200 μm it is resolved by the numerical solution of the heat equation. It can be seen from Fig. 3(b) that for the present film thickness of 200 μm, the portion of the total supercooling contained within the film increases with tip speed. For example, for a tip speed of 85 μm/s about 70% of the total supercooling of 0.8 K is contained within the film, while the remainder is outside the confocal envelope where it is resolved by the numerical solution. For a total supercooling of 0.2 K, the portion contained within the film is less than 20%. Despite these variations in the partitioning of the supercooling, the tip velocities are predicted well, as discussed above.

While the above comparison establishes the minimum film thickness needed to predict the correct tip speeds, it does not address the ability of the mesoscopic model to predict the thermal interactions between adjacent dendrite branches and produce a realistic grain envelope shape. The establishment of the grain envelope shape is illustrated in Fig. 4. The calculations are started with a spherical grain envelope that has a radius approximately equal to the film thickness. Figure 4(a) shows the octahedral envelope that is predicted by the envelope propagation algorithm when the same tip speed (50 μm/s) is used everywhere. In other words, the octahedral shape results when the envelope propagation algorithm is decoupled from the numerical solution of the heat equation and the confocal envelope temperature (0.4 K here) is uniform around the grain.

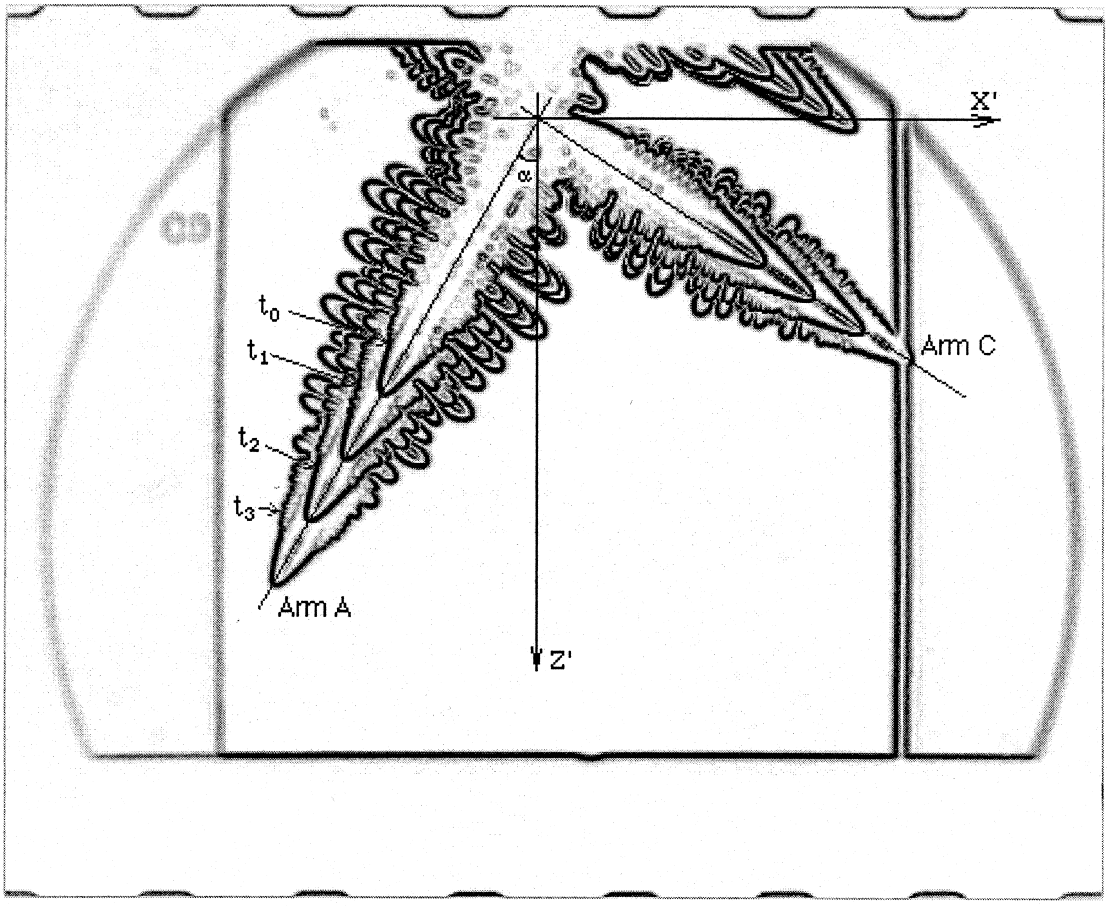

Fig. 5. Superimposed SCN dendrite images taken at four different times during the IDGE microgravity experiment of Glicksman and coworkers [11–13] flown on the USMP-2 mission (ΔT = 0.370 K); the time interval between the images is 83.25 s.

It can be seen that the algorithm produces the expected shape.

The corresponding solution, where the full mesoscopic model is solved and the envelope propagation algorithm is coupled to the numerical solution of the heat equation, is shown in Fig. 4(b)–(d). Due to reduced heat fluxes at the faces of the octahedron, compared to the corners, the temperatures of the confocal grain envelope there are closer to the melting temperature, resulting in lower supercoolings and growth speeds at the faces. Conversely, the heat fluxes from the corners are greater, resulting in lower confocal envelope temperatures and higher tip speeds. Consequently, a realistic looking equiaxed grain envelope evolves that has six primary branches at right angles. Figure 4(d) shows a cut through one of the primary branches. Due to different heat fluxes at the edges and sides and, hence, different speeds of the secondary and tertiary dendrite arm tips, a realistic looking cross-sectional shape evolves. A detailed experimental validation of the predicted envelope shape is provided in the Section 5.

5. EXPERIMENTAL VALIDATION FOR A SINGLE GRAIN

The mesoscopic model is validated for a single equiaxed dendritic grain by comparing predicted grain envelope shapes and solid fractions to measurements from an experiment involving diffusion-controlled growth of a pure substance in a uniformly supercooled melt. The experiment is the Isothermal Dendritic Growth Experiment (IDGE) of Glicksman and coworkers [11–13], launched on the space shuttle by NASA in March 1994 as part of the United States Microgravity Payload (USMP-2). The IDGE uses pure SCN which is contained inside a temperature-controlled growth chamber. After melting the SCN and establishing the desired supercooling level, the growth of a dendrite is initiated on a stinger by activating a thermoelectric

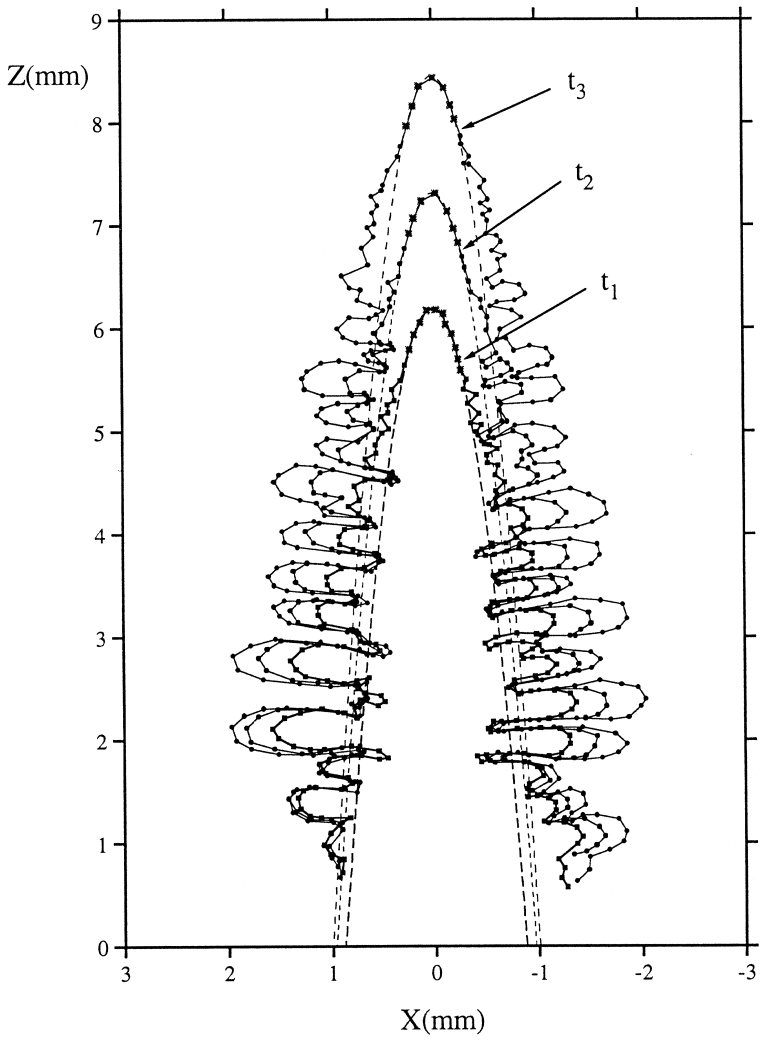

Fig. 6. Dendrite arm A reconstructed from the superimposed images in Fig. 5 and rotated to lie in a side-branch plane; the interrupted lines are the parabolas fitted to the tip.

cooler. During growth, photographs are taken at regular time intervals along two perpendicular optical paths. The image analysis techniques used to extract the desired data from the photographs are described in detail in Ref. [14].

Figure 5 shows four superimposed images taken at different times during one of the experimental runs. The orientation of the dendrite is determined and the solid/liquid interface is tracked by marking it with a sufficient number of points. Then, the coordinates of the points are transformed by rotation and translation, such that the side-branch plane of interest is placed in the X–Z plane of reference and the symmetry axis of the dendrite arm is oriented along the Z-axis. An example is shown in Fig. 6. The envelope shape is obtained by measuring the distance, X_{tip}, of the active secondary side-branch tips from the primary axis as a function of the distance, Z, from the primary tip. Again, a branch is judged active when it is longer than the next active branch closer to the primary tip.

Figure 7 shows measured active secondary tip positions obtained from experimental runs at four different supercoolings (ΔT = 0.287 K, 0.370 K, 0.470 K, and 0.609 K). By normalizing the lengths by the primary dendrite tip radius, R, all data obtained at various times during growth and the four supercooling levels collapse along a single line, indicating self-similar growth behavior for the envelope shape. Ignoring the data in the primary tip region ($Z/R < 10$), the branch tip positions and, hence, the envelope shape are correlated by

$$\frac{X_{\text{tip}}}{R} = 0.668\left(\frac{Z}{R}\right)^{0.859} \tag{11}$$

This experimental correlation is valid in the self-similar regime given by $1 \ll Z/R \ll 1/Pe$, where Pe is the tip Peclet number as defined above [14].

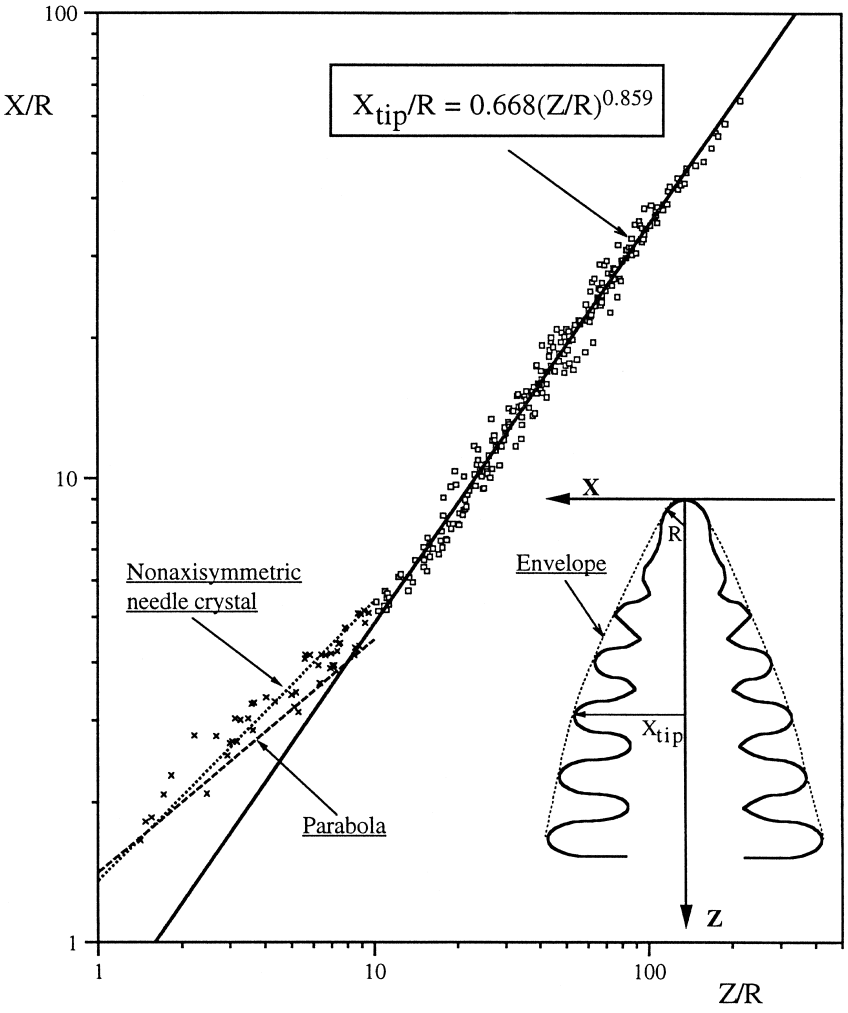

Fig. 7. Experimental scaling relation between the normalized envelope width X/R and the normalized distance away from the primary tip, Z/R; the symbols represent all data obtained at different times for both sides of a dendrite at four different supercooling levels (ΔT = 0.287, 0.370, 0.470 and 0.609 K); only the squares were used in fitting the scaling relation.

The image analysis procedures used to measure the solid volume of the dendrites from the IDGE photographs are also explained in Ref. [14]. The solid volumes are converted to mean solid fractions for an entire equiaxed grain by multiplying the volume of a primary branch by six and dividing it by the volume of a certain grain envelope. In order to avoid any ambiguities related to the envelope shape, the mean solid fraction, $\bar{f}_s$, is defined here for a spherical envelope having a radius equal to the primary arm length Z. The resulting experimental correlation is given by [14]

$$\bar{f}_s = 3.86\left(\frac{Z}{R}\right)^{-0.90} \tag{12}$$

which again is only valid in the self-similar regime $1 \ll Z/R \ll 1/Pe$. For $Z/R > 1/Pe$, the mean solid fraction approaches the dimensionless supercooling $\Delta T/(L/c)$. Note that the axial coordinate Z/R can also be interpreted as a dimensionless time $\tau = t \cdot v/R = Z/R$, where t is the time.

The above two experimental correlations are now used to validate the mesoscopic model predictions. Figure 8 compares the envelope shapes for a primary branch predicted for three supercoolings (symbols) to the experimental correlation given by equation (10) (line). The agreement is reasonably good, keeping in mind that the envelope shape in the simulations is not prescribed but is a result of the coupling of the microscopic growth model to the mesoscopic temperature field around the envelope. In the simulations, the dendrite arms were grown to the same length (in dimensional coordinates) for all supercoolings. Then, the scaling of the lengths with the tip radius in Fig. 8 results in the predicted envelopes appearing shorter with decreasing supercooling. It can be seen from Fig. 8 that the mesoscopic model somewhat overpredicts the envelope width for the highest supercooling. This disagreement is of the same origin as the slight

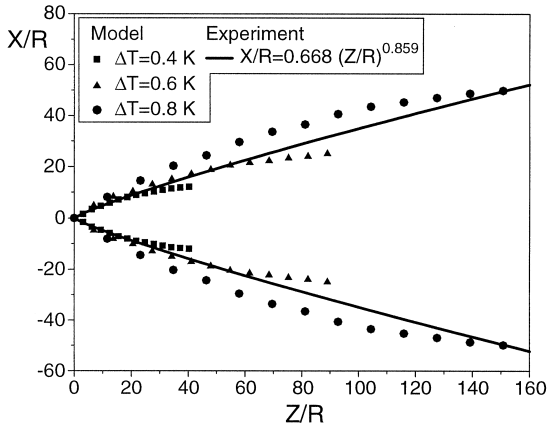

Fig. 8. Comparison of the predicted envelope shape with the experimental scaling relation, equation (10), for three different supercoolings.

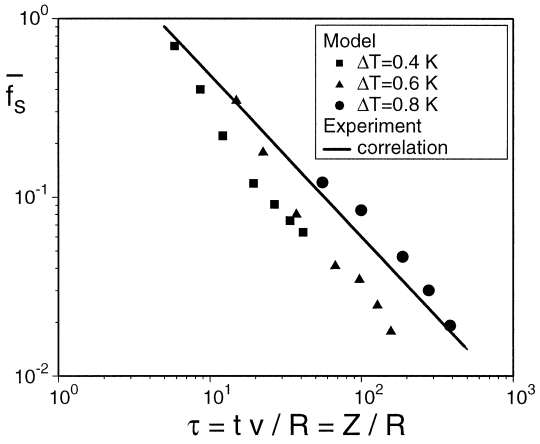

Fig. 9. Comparison of predicted mean solid fractions in a spherical envelope for different supercoolings (symbols) with the experimental scaling relation, equation (11).

overprediction of the tip velocity for the higher supercoolings in Fig. 3(a) and (b): the stagnant-film thickness (of 200 μm) is becoming too large relative to the tip radius. Figure 8 also shows that the envelope width for the lower supercoolings is underpredicted in the dendrite root region, away from the tip. In the root region, the local supercooling in front of the secondary dendrite tips is very small (below 0.1 K) resulting in the film thickness becoming too small relative to the tip radii. In summary, the above comparison indicates that it is generally important to ensure that everywhere on the envelope the film thickness is of the same order of magnitude as, but larger than, the tip radii. However, reasonably accurate results can be obtained with the same film thickness for a range of growth conditions.

Figure 9 shows that reasonable agreement also exists between the measured and predicted mean solid fraction evolution, further validating the mesoscopic model. The solid fraction predictions for the lower two supercoolings are somewhat

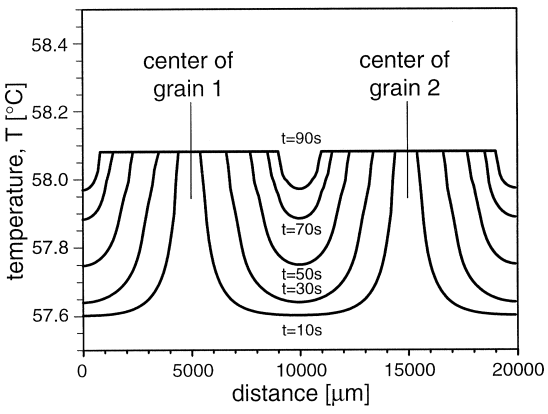

Fig. 10. Predicted evolution of the temperature distribution between two dendrite branches approaching each other ($\Delta T_i = 0.48S$ K, SCN).

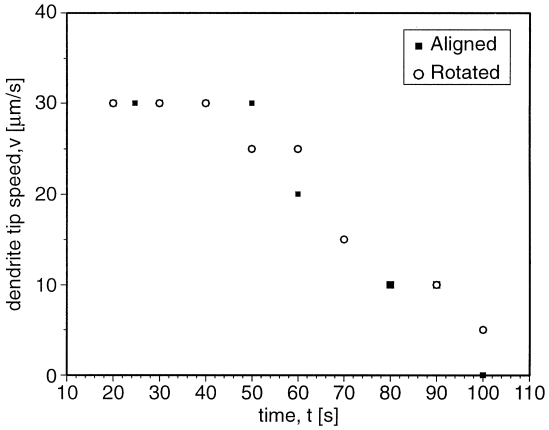

Fig. 11. Predicted evolution of the tip speeds for a dendrite branch approaching another grain; results are shown for the aligned case corresponding to Fig. 10 for the first 100 s (filled symbols) and another case where the reference grain is rotated by 45° (open symbols) ($\Delta T_i = 0.48$ K, SCN).

lower than the experimental correlation, which can be explained by limitations associated with the numerical grid used. In the calculations, the grain evolves from a spherical seed that must have a minimum radius of about two grid spacings (i.e. 200 µm). This seed size is too large compared to the grain sizes expected in the self-similar regime. Either a finer grid or an improved seeding procedure will be implemented in the near future.

6. RESULTS FOR MULTIPLE GRAINS

In this section, we present several examples of simulations involving multiple equiaxed grains. As a first step, the growth of two interacting grains is examined. The initial supercooling is 0.48 K and the center-to-center distance between the grains is 10 mm. Figure 10 plots the temperature distribution at different times between the tips of two grains with aligned growth directions (i.e. the tips grow directly toward each other). Until 40 s, the tips grow uncoupled. Thereafter, the temperature fields significantly overlap. Figure 11 plots the evolution of the tip speed for the aligned case as well as for a case, where the second grain was rotated by 45° with respect to the first grain. Due to the interactions, the speed reduces to zero at about 100 s. In the case where the second grain is rotated such that the reference tip points into the region between primary branches, the final growth stage is slightly prolonged.

Another simulation is performed with four grains, located at the corners of a tetrahedron. The nuclei are oriented randomly at a distance of about 4 mm from each other. Figure 12 shows dendrite envelopes for the four grains at two different times. The outpointing branches are much more elongated than the branches pointing into the center of the box, because the outpointing branches have more

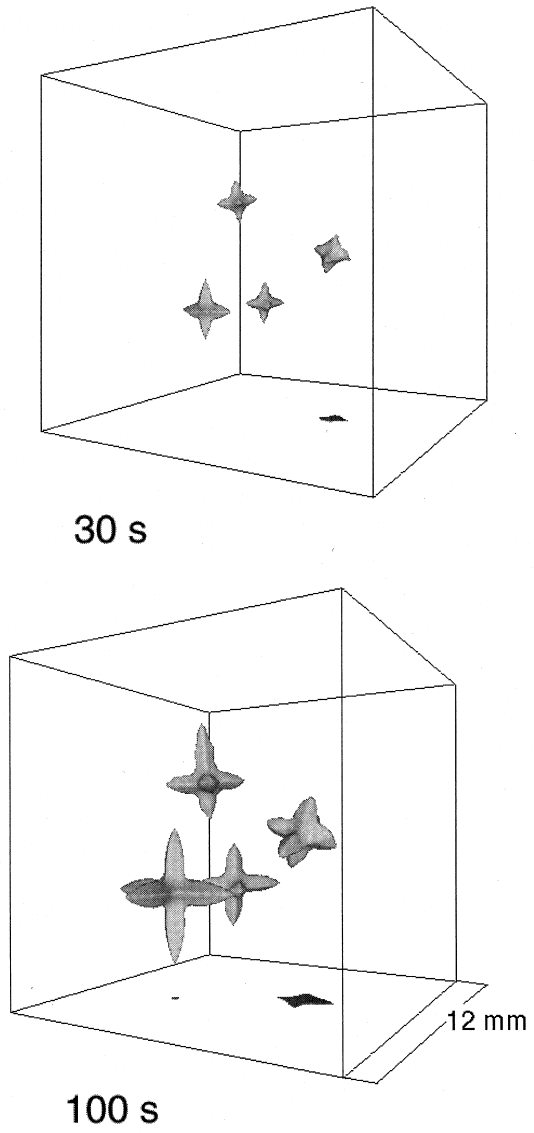

Fig. 12. Predicted envelope shapes of four equiaxed dendritic grains centered at the corners of a tetrahedron (equal distances of about 4 mm) at 30 s and 100 s after seeding ($\Delta T_i = 0.48$ K, SCN).

favorable conditions to grow. The inward pointing branches grow more slowly because of thermal interactions between the grains.

Finally the growth of 14 grains is simulated for two different seeding configurations. The results for the grain envelopes are shown in Fig. 13. The ordered configuration shows an overall faster growth than the random configuration due to better filling of the space in the ordered case. While the above results for multiple grains need to be analyzed in more detail and also require experimental validation, they illustrate the capabilities of the present model. The number of numerical grid points used in these calculations is $120 \times 120 \times 120$, and the grid size is $dx = dy = dz = 100$ µm. The

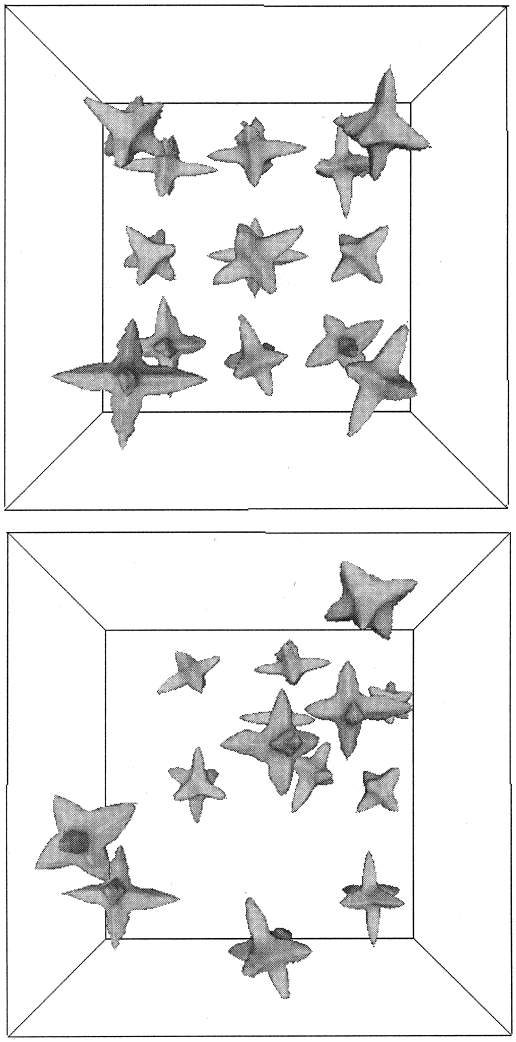

Fig. 13. Examples of predicted envelope shapes of 14 equiaxed dendritic grains; the upper panel corresponds to an ordered arrangement of seeds, while the lower panel shows a random configuration.

calculations require of the order of 4.5 CPU hours on a 100 MFlops workstation.

7. CONCLUSIONS

The growth of multiple equiaxed dendrites of a pure substance growing in a supercooled melt is modeled using a novel mesoscopic simulation technique. The model couples the solution of the heat diffusion equation in the supercooled melt around the equiaxed grain envelopes with a local analytical solution (i.e. the stagnant-film model) for calculating the dendrite tip speeds. It allows for the prediction of the evolution of the grain envelope shape and the internal solid fraction. The model is successfully validated for the case of a single grain through a comparison of the predictions with experimental measurements from the IDGE.

Several simulation results for the growth of multiple grains are presented in order to illustrate the model capabilities. They reveal the transient variations in the growth speeds and the development of asymmetric grain shapes due to thermal interactions between the grains. Future work will include a more detailed analysis and experimental verification of these and other results. We envision that the basic modeling concept presented here can be extended to simulate columnar dendritic growth, grain structure transitions, solutal transport, and even growth in the presence of melt flow.

Acknowledgements—The authors I. Steinbach and B. Kauerauf were supported by DARA under grant WS-50WM9565. The authors C. Beckermann, Q. Li and J. Guo were supported by NASA under grant NCC8-94.

REFERENCES

1. Flemings, M. C., *Solidification Processing*. McGraw-Hill, New York, 1974.
2. Beckermann, C. and Wang, C. Y., in *Annual Review of Heat Transfer*, Vol. 6, ed. C. L. Tien. Begell House, New York, 1995, pp. 115–198.
3. Caroli, B. and Müller-Krumbhaar, H., *Iron Steel Inst. Japan Int*., 1995, **35**, 1541.
4. Karma, A. and Rappel, W., *Phys. Rev. Lett*., 1996, **77**, 4050.
5. Rappaz, M. and Thevoz, Ph., *Acta metall*., 1987, **35**, 1487.
6. Gandin, Ch. A. and Rappaz, M., *Acta metall*., 1994, **42**, 2233.
7. Steinbach, I., Kauerauf, B., Beckermann, C. and Guo, J., in *Solidification 1998*, ed. S. P. Marsh *et al*. TMS, Warrendale, P A, 1998, pp. 5–14.
8. Hinze, J. O., *Turbulence*. McGraw-Hill, New York, 1975.
9. Cantor, B. and Vogel, A., *J. Cryst. Growth*, 1977, **14**, 109.
10. Diepers, H. J., Beckermann, C. and Steinbach, I., in *Solidification Processing 1997*, ed. J. Beech and H. Jones. SRP Ltd., Exeter, U.K., 1997, pp. 426–430.
11. Glicksman, M. E., Winsa, E. A., Hahn, R. C., LoGrasso, T. A., Tirmizi, S. H. and Selleck, M. E., *Metall. Trans*., 1988, **19A**, 1945.
12. Glicksman, M. E., Koss, M. B., Bushnell, L. T., LaCombe, J. C., Smith, R. N. and Winsa, E. A., in *Heat Transfer in Microgravity Systems*, Vol. 290, ed. S. S. Sadhal and A. Gopinath. ASME, New York, 1994, p. 1.
13. LaCombe, J.C., Koss, M.B., Fradhov, V.E. and Glicksman, M.E., *Phys. Rev. E*, 1995, **52**, 2778.
14. Li, Q. and Beckermann, C., *Phys. Rev. E*, 1998, **57**, 56.